Supporting Information

Effect of Structural Phase Transition on Charge-Carrier Lifetimes and Defects in $CH_3NH_3SnI_3$ Perovskite

Elizabeth S. Parrott, Rebecca L. Milot, Thomas Stergiopoulos, Henry J. Snaith, Michael B. Johnston, Laura M. Herz.*

Department of Physics, University of Oxford, Clarendon Laboratory, Parks Road, Oxford OX1 3PU, UK

*laura.herz@physics.ox.ac.uk

Experimental Methods

Sample fabrication

To form the perovskite precursor solution, tin(II) acetate (Sigma) and methylammonium iodide (Dyesol) were dissolved in anhydrous N,N-Dimethylformamide (DMF) at a 3:1 molar ratio with final perovskite precursor concentration of ~30 wt%. Clear yellow solution was obtained by filtering the turbid solution using a PTFE filter (pore size of 0.45 μm). Then, the solution was spin-coated at 6000 rpm (for 45 s) with a ramp-up of 6000 rpm s^{-1}. After spin-coating, the dark brown films were left to dry at room temperature for around 5 minutes and then annealed at 130°C for 2 minutes to become black. Every step was performed in a nitrogen-filled glovebox.

Photoluminescence spectra

Samples were excited using a tunable Ti:Sapphire pulsed (80 fs) laser with a wavelength of 800 nm and an 80 MHz repetition rate (Mai Tai, Spectra-Physics). A BBO crystal was used to double the excitation frequency, giving a wavelength of 400 nm. The 800 nm fundamental wavelength was filtered out using a polariser and a colour filter. The excitation intensity was attenuated down to 500 μW over an area of 0.2 mm^2 to give a fluence of approximately 3 $nJcm^{-2}$ using an OD1 filter and a variable attenuator consisting of a waveplate and a vertical polariser. A horizontal polariser and a 550-nm long-pass colour filter were placed after the sample to remove any laser scatter from the spectrum. Samples were fabricated inside a nitrogen filled glovebox and sealed inside a cold-finger cryostat (MicrostatHe, Oxford Instruments) whilst still inside the glovebox to eliminate exposure to air. The cryostat was then transferred to the laser laboratory and evacuated, maintaining a pressure below 10^{-5} mbar, with no degradation in PL observed for

the duration of the measurements. The temperature was controlled by a flow of liquid helium and an electronic temperature controller (ITC503, Oxford Instruments). The temperature was monitored with sensors both on the cryostat heat exchanger and the end of the sample holder. Photoluminescence from the sample was collected by a pair of off-axis parabolic mirrors and focused onto the entry slit of a grating monochromator (Triax, Horiba). The spectrally resolved PL was detected by a nitrogen-cooled Si-CCD detector (Symphony, Horiba) and the spectral response of all components was corrected for using a tungsten filament lamp with known spectrum. This is particularly important for tin perovskites since the sensitivity of the CCD drops off in the NIR where these materials emit.

Time-resolved photoluminescence

The set up for time-resolved photoluminescence was the same as above, except that light emitted at the peak PL wavelength was selected by a second slit and detected by a silicon single photon avalanche diode used for time correlated single photon counting (TCSPC). The instrument response function was measured by tuning the (80-fs pulsed) laser to 990 nm and measuring the response due to laser scatter from a roughened quartz disk placed in the sample holder. The detector response is slightly dependent on detection wavelength, so 990 nm was chosen to be close to the wavelength of the PL.

Absorption

Visible to near infrared (NIR) transmission measurements were performed using a Fourier transform infrared spectrometer (Vertex 80v, Bruker). A tungsten halogen lamp was used as a light source, and the light passing through the sample was detected by a silicon diode detector

and compared with a blank substrate to determine the fraction transmitted at a given wavelength (T). Since the material has relatively little reflection or diffuse scattering, the absorption at a given wavelength (A) was determined by A = 1 - T. The cryostat used for the photoluminescence measurements was also used here, but due to the configuration of the system, the samples had to be exposed to air for about a minute during transfer before being measured under vacuum.

Fit to room temperature PL decay curve

The measured decay curve (MD) and IRF were smoothed and then deconvoluted to produce the real decay curve (RD) according to the formula

$$F(MD) = F(IRF)F(RD)$$

$$RD = F^{-1}\left[\frac{F(MD)}{F(IRF)}\right]$$

where F and F^{-1} are the Fourier transform and inverse Fourier transform respectively. We then calculated the time for RD to drop to 1/e of its maximum value.

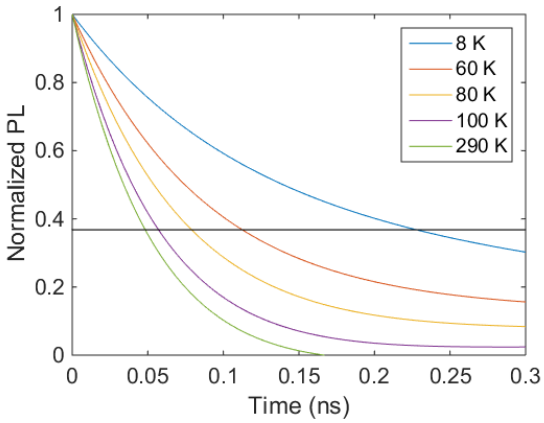

Figure S1. Real decay curves determined by smoothing the measured decay curves and deconvolving with the instrument response function. The horizontal line marks 1/e.

Additional results

Gaussian Fits of Spectra

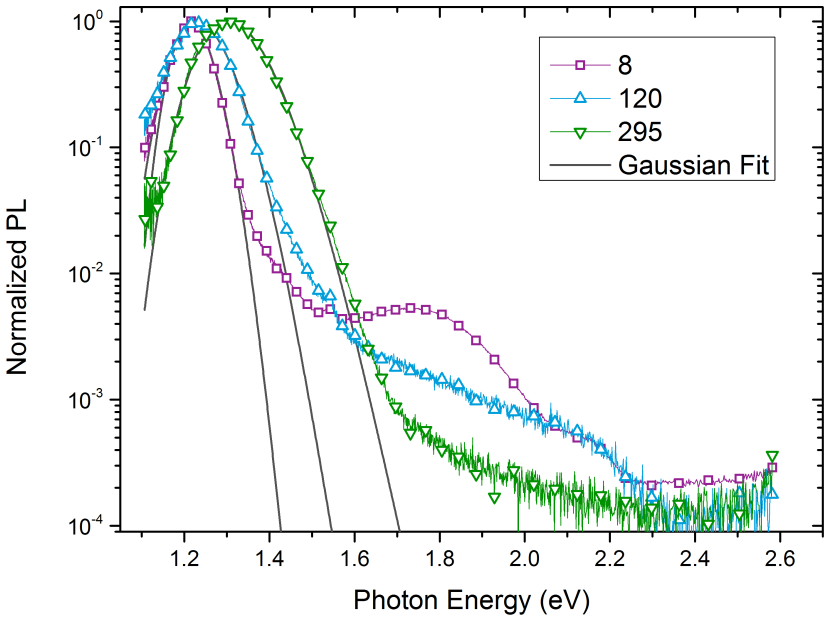

Figure S2. Examples of Gaussian fits used to determine peak PL and FWHM

Time-resolved PL of secondary transition

Decay curves for the PL at both the main peak (T1) and the secondary peak (T2) at 8 K are shown in Figure S3 for two different fluences (30 and 300 nJcm^{-2}). At the lower fluence (3 nJcm^{-2}), used in the rest of the measurements presented in the main text, the signal-to-noise ratio for the secondary peak (T2) is poor. For the highest fluence, the initial decay of the secondary peak (T2) PL is limited by the IRF and is therefore too fast for the resolution of the system. Such rapid dynamics could be the result of fast interband relaxation. There is also a longer lived component, that could potentially arise from overlapping PL from T1.

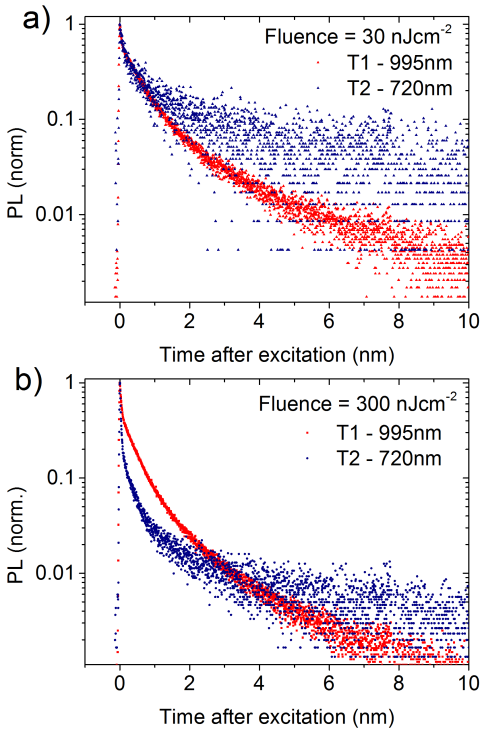

Figure S3. Time-resolved photoluminescence of the two peaks at 8K at (a) low fluence and (b) high fluence.

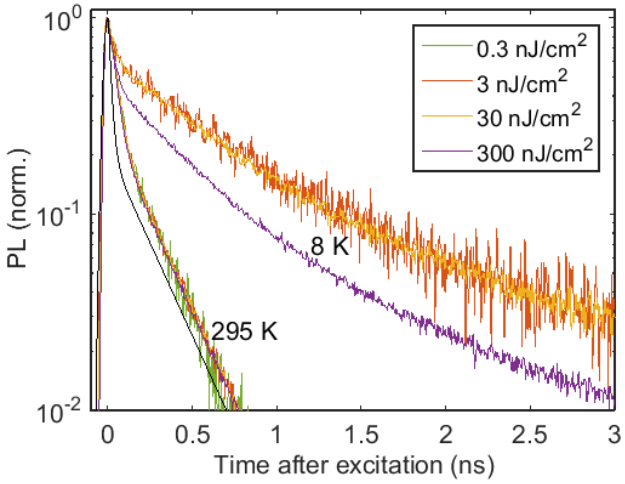

Figure S4. Fluence dependence of the PL decay curve at room temperature and low temperature. The black curve is the IRF.

Schematic: Origin of transition T2

As discussed in the main text, the secondary absorption onset and PL are likely to be due to a band to band transition T2. Possibilities include A, a transition to the spin-orbit split conduction band[1], B, a transition to a second valence band (previously suggested in $MAPbI_3$)[2] and C, a transition at a different point in k-space, shown in Figure S5. The bands shown are illustrative since calculations for this material are limited.[3,4]

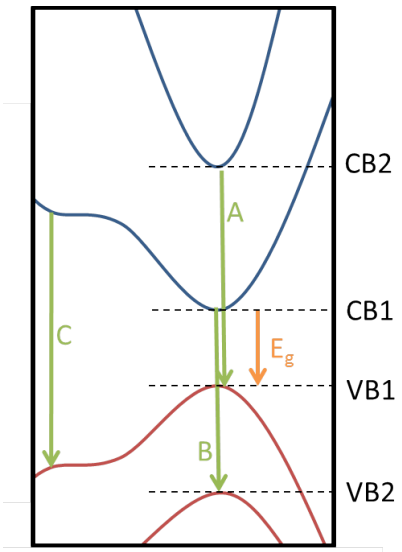

Figure S5. A schematic band dispersion diagram showing possible transitions responsible for T2.

Temperature dependence of linewidth

Figure S6 shows the functional form of each term in the model of temperature dependent photoluminescence linewidth described by the equation[5]

$$\Gamma(T) = \Gamma_{ac} + \Gamma_{LO} + \Gamma_{imp} + \Gamma_{\circ}$$

where the contributions to the broadening are from acoustic phonons $\Gamma_{ac} = \gamma_{ac}T$, longitudinal optical phonons $\Gamma_{LO} = \gamma_{LO} / (e^{E_{LO}/kT} - 1)$, ionized impurities $\Gamma_{imp} = \gamma_{imp}\, e^{-E_b/kT}$ and energetic

disorder Γ_0. At high temperature both phonon terms give a linewidth directly proportional to temperature whereas the ionized defect term has a sublinear temperature dependence.

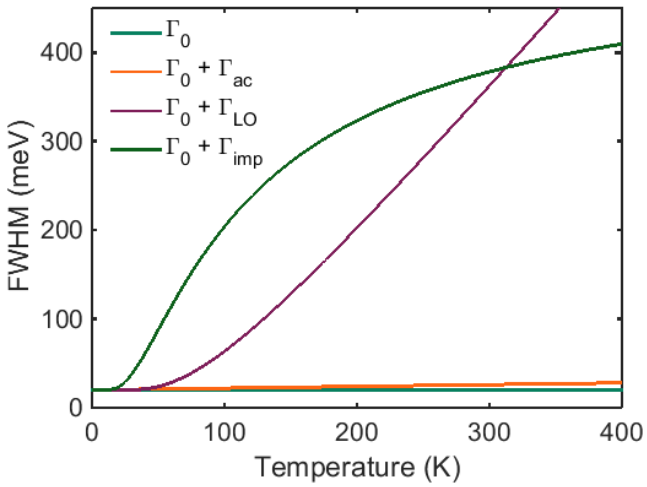

Figure S6. Temperature dependence of the four terms in the line width model. Values are illustrative only and not fits to the data: Γ_0 = 20 meV, γ_{ac} = 0.02 meV/K, γ_{LO} = 400 meV, E_{LO} = 20 meV, γ_{imp} = 500 meV, E_b = 100 meV.

Since we believe there to be a change to the impurity levels at the phase transition we may only fit this model to our data within one structural phase. Data within the low temperature phase varies too little to produce a meaningful fit but we are able to fit the data within the tetragonal phase in the region 140-270 K. The linewidth is dominated by impurity scattering so we neglect the phonon terms, leaving

$$\Gamma(T) = \gamma_{imp}\, e^{-E_b/kT} + \Gamma_0$$

The best fit gives a donor-carrier binding energy of 10 meV, but since the temperature range over which we are fitting is small we cannot determine the value accurately, and binding energies up to 20 meV are plausible.

Phonons at high temperatures can be accounted for by adding a linear term αT where $\alpha = \gamma_{ac} + k.\gamma_{LO}/E_{LO}$, however, adding such terms to the fitting function does not significantly alter the estimate of the binding energy in agreement with our notion that the linewidth is dominated by charge-carrier scattering with impurities within this temperature regime.

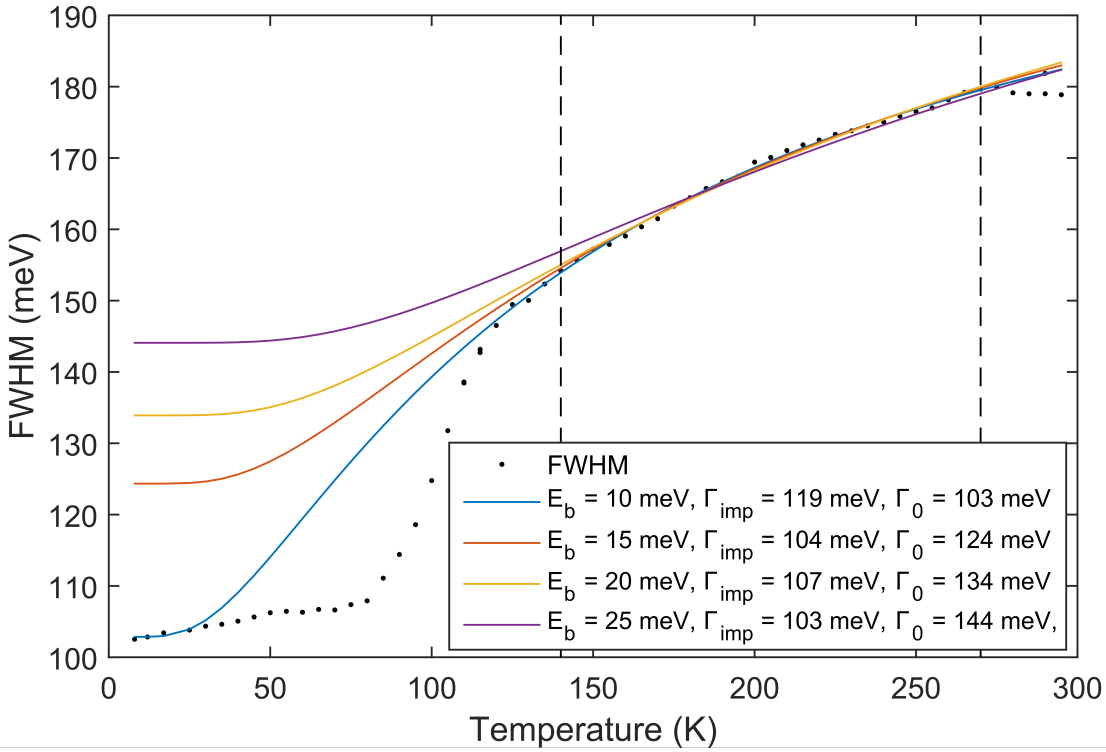

Figure S7. Plausible fits to the PL FWHM data within the dashed region (140-270 K) giving different binding energies. For the 25 meV fit, the binding energy had to be fixed at this value which shows that binding energy values above 20 meV do not describe the data well.

References

(1) Even, J.; Pedesseau, L.; Jancu, J.-M.; Katan, C. DFT and k·p Modelling of the Phase Transitions of Lead and Tin Halide Perovskites for Photovoltaic Cells. *Phys. status solidi - Rapid Res. Lett.* **2014**, *8*, 31–35.

(2) Xing, G.; Mathews, N.; Sun, S.; Lim, S. S.; Lam, Y. M.; Grätzel, M.; Mhaisalkar, S.; Sum, T. C. Long-Range Balanced Electron- and Hole-Transport Lengths in Organic-Inorganic $CH_3NH_3PbI_3$. *Science* **2013**, *342*, 344–347.

(3) Takahashi, Y.; Hasegawa, H.; Takahashi, Y.; Inabe, T. Hall Mobility in Tin Iodide

Perovskite $CH_3NH_3SnI_3$: Evidence for a Doped Semiconductor. *J. Solid State Chem.* **2013**, *205*, 39–43.

(4) Even, J.; Pedesseau, L.; Katan, C.; Kepenekian, M.; Lauret, J.-S.; Sapori, D.; Deleporte, E. Solid State Physics Perspective on Hybrid Perovskite Semiconductors. *J. Phys. Chem. C* **2015**, *119*, 10161–10177.

(5) Chen, Y.; Kothiyal, G. P.; Singh, J.; Bhattacharya, P. K. Absorption and Photoluminescence Studies of the Temperature Dependence of Exciton Life Time in Lattice-Matched and Strained Quantum Well Systems. *Superlattices Microstruct.* **1987**, *3*, 657–664.